Absorption imaging of trapped 1*s* paraexcitons in bulk Cu_2O

Kosuke Yoshioka[1] and Makoto Kuwata-Gonokami[1,2,*]

[1]*Department of Physics, Graduate School of Science, The University of Tokyo, 7-3-1 Hongo, Bunkyo-ku, Tokyo 113-0033, Japan*

[2]*Photon Science Center, Graduate School of Engineering, The University of Tokyo, 7-3-1 Hongo, Bunkyo-ku, Tokyo 113-8656, Japan*

(Received 30 December 2014; revised manuscript received 11 May 2015; published 27 May 2015)

We demonstrate absorption imaging of 1*s* paraexcitons in a strain-induced trap potential in bulk semiconductor Cu_2O. Using excitonic 1*s*-2*p* induced absorption in the midinfrared region, clear images of exciton ensembles are taken at liquid-helium temperatures. The observed spatial spread and redshift of the 1*s*-2*p* resonance prove that the images are of a thermalized gas of trapped 1*s* paraexcitons. With its high sensitivity, midinfrared absorption imaging is especially important for characterizing quantum degenerate paraexcitons including Bose-Einstein condensates at near 100 mK temperatures, as they do not luminesce because of the principle of momentum conservation.

DOI: 10.1103/PhysRevB.91.195207 PACS number(s): 78.40.Fy, 42.62.Fi, 71.35.Cc, 78.47.−p

Experiments on the Bose-Einstein condensation (BEC) of excitons in bulk Cu_2O have recently been extended to sub-Kelvin temperatures. Due to their decoupling from the radiation field, the long-lived 1*s* paraexcitons in Cu_2O are expected to form a matterlike three-dimensional (3D) BEC, making the elementary excitations unique. However, the system has large exciton-exciton collision-induced loss coefficients [1–5], resulting in a reduction of the critical density and hence the critical temperature below 1 K. At an exciton temperature of 800 mK, indirect evidence of the BEC transition was found [6] in a strain-induced trap [7,8].

Experiments using a dilution refrigerator have been performed [9,10] to set a lower critical density for preparing a stable BEC by further cooling the Cu_2O crystals. We experimentally demonstrated that the exciton temperature reached a promising sub-100-mK region because the activation of interactions between paraexcitons and transverse acoustic phonons took place in a strain-induced trap [9]. The importance of the exciton-exciton elastic scattering for thermalization at such ultralow temperatures has also recently been discussed theoretically [11].

Although the cooling and trapping methods have been established for creating a stable BEC, a major problem arises when observing the ultracold paraexciton gas. As discussed below, the direct recombination process, which has been used to monitor the spatial and spectral distribution of trapped paraexciton gases, becomes forbidden if the exciton temperature is less than about 120 mK. Hence, it is indispensable to develop an alternative method for detecting such dark excitons at ultralow temperatures directly, to find conclusive evidence for the quantum statistics and BEC of the photoexcited quasiparticles.

Here, we propose that "excitonic Lyman spectroscopy" (which uses the 1*s*-2*p* transition of excitons) can overcome the aforementioned difficulty. This spectroscopic method has been developed as a quantitative probe for dark paraexcitons in strain-free samples [1,12–17]. The excitonic 1*s*-2*p* induced absorption spectrum in the midinfrared region gives a direct measure of the absolute number and thermal distribution of 1*s* excitons. If absorption imaging of trapped excitons can be realized using this method, as is routinely done in cold-atom experiments [18–20], a minute investigation of the spatial and momentum distribution of the exciton gas will enable us to precisely evaluate the thermal distribution of the gas and to provide direct evidence for BEC. To that end, it is necessary to investigate the applicability of excitonic Lyman spectroscopy in a strain-induced trap, and to report the influence of the inhomogeneous strain field on the 1*s*-2*p* resonance.

In this paper, we demonstrate the absorption imaging of trapped 1*s* paraexcitons in a three-dimensional trap at liquid-helium temperature, and show that absorption imaging has sufficient sensitivity to observe relatively low-density paraexcitons that are required for BEC experiments at 100 mK temperatures. Together with the ability to measure the spatial and the spectral distributions of the trapped exciton gas shown here, the absorption imaging technique will serve as a primary tool for visualizing either trapped or untrapped dark exciton gases. The idea can be extended to other exciton systems in general, by applying appropriate THz probe electromagnetic waves.

The direct recombination process is strictly forbidden for 1*s* paraexcitons in a strain-free crystal. In a strain field, however, the recombination process becomes slightly allowed, and paraexcitons that have a specific momentum [which is determined by the intersection between the dispersion relations of the 1*s* paraexcitons, $E(k) = E_0 + \hbar^2 k^2/(2m_{1s})$, and the photons, $E(k) = \hbar ck/n$] contribute to the luminescence, as depicted in Fig. 1(a). $E_0 = 2.0215$ eV (in a strain-free crystal, as an example) is the strain-dependent energy of the 1*s* paraexciton state at zero momentum, $m_{1s} = 2.6m_0$ [21,22] is the effective mass of 1*s* paraexcitons (m_0 is the electron mass at rest), and $n = 2.55$ is the index of refraction of the Cu_2O crystal. The very small damping of the paraexciton state and the very small oscillator strength of the quadrupole transition to the ground state even in a magnetic field [23] assure the validity of this picture. The corresponding wave number of the intersection is $k_0 = 2.6 \times 10^7$ m^{-1}, and the corresponding kinetic energy of the paraexcitons is $\Delta = 10\ \mu$eV. The equivalent exciton temperature is 120 mK, and it is at this temperature that the momentum-dependent forbidden nature takes effect.

In general, a Γ_5^--LO-phonon-assisted, indirect recombination process is allowed as a momentum-independent luminescence channel for 1*s* paraexcitons. In practice, how-

*gonokami@phys.s.u-tokyo.ac.jp

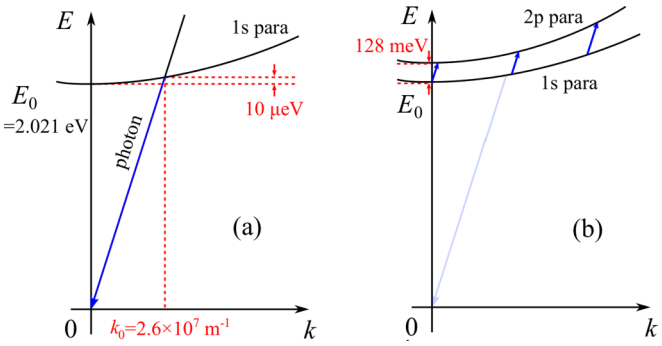

FIG. 1. (Color online) (a) The radiative recombination process due to the direct transition that is slightly allowed in a strain field. Paraexcitons at the intersection with the dispersion relation of photons can contribute to the photon emission (see text). Paraexcitons that have a translational kinetic energy of less than 10 μeV (120 mK) in a trap have zero possibility to be at the intersection. (b) In the excitonic $1s$-$2p$ (Lyman-α) transition, the final state is prepared even for $1s$ paraexcitons with the zero momentum state (BEC).

ever, it is impossible to characterize the ultracold excitons via phonon-assisted luminescence for the following reasons: (1) Due to the very small transition probability, the total luminescence signal from a low-density exciton gas does not provide a good enough signal-to-noise ratio for estimating the spatial and spectral distribution, or for measuring absolute luminescence [1–3] for reliable calibration of the density. (2) It is hard to distinguish paraexcitons from the adjacent, LO-phonon-assisted luminescence of orthoexcitons that is orders of magnitude stronger.

Conversely, excitonic Lyman spectroscopy [Fig. 1(b)] utilizes a dipole-allowed (even for BEC), strong transition at about 128 meV. Therefore, it can be used to estimate the absolute density of $1s$ paraexcitons from the magnitude of the induced infrared absorption. In addition, the spectrum of the induced absorption reflects the momentum distribution of the $1s$ excitons because of the difference between the masses of the $1s$ and $2p$ excitons ($m_{1s} = 2.6m_0$, $m_{2p} = 1.68m_0$). Full characterization of the trapped $1s$ paraexciton gas is possible if we extend this method to the evaluation of the spatial distribution.

Figure 2 is a schematic of our setup. The sample is a natural single crystal of Cu_2O (5.3 × 5.3 × 9 mm). We applied stress along the [001] crystal axis using a BK7 spherical singlet lens with a radius of curvature of 7.79 mm. The induced inhomogeneous strain distribution gave a position-dependent shift of the paraexciton level and thus formed a three-dimensional trap potential [7,8]. We cooled the sample using liquid helium. The thermometer of the heat exchanger in our continuous-flow cryostat indicated a temperature of 2.3–2.4 K, but the temperature of the crystal could be significantly higher because the windows fully transmitted high-power thermal radiation at room temperature. The excitation laser was a continuous-wave dye laser at 606.2 nm. A single-mode fiber served as a transverse-mode cleaner. The typical excitation power inside the crystal was 10 mW, and it was intensity stabilized. About 30% of the incident laser beam was absorbed around the trap potential via a LO-phonon-assisted absorption process of $1s$ orthoexcitons. The generated $1s$ orthoexcitons converted into $1s$ paraexcitons within 1 ns and they accumulated at the trap potential. The exciton gas was completely in the classical regime, and in thermal equilibrium.

We sent the probe beam in a perpendicular direction to the excitation beam. The probe beam was provided by a tunable, single longitudinal mode quantum cascade laser. We attached a circular aperture with a 1 mm diameter as a guide for the midinfrared radiation. The trap region was magnified by 7.8 times using a pair of lenses, and we performed a raster scan using a nitrogen-cooled HgCdTe (mercury

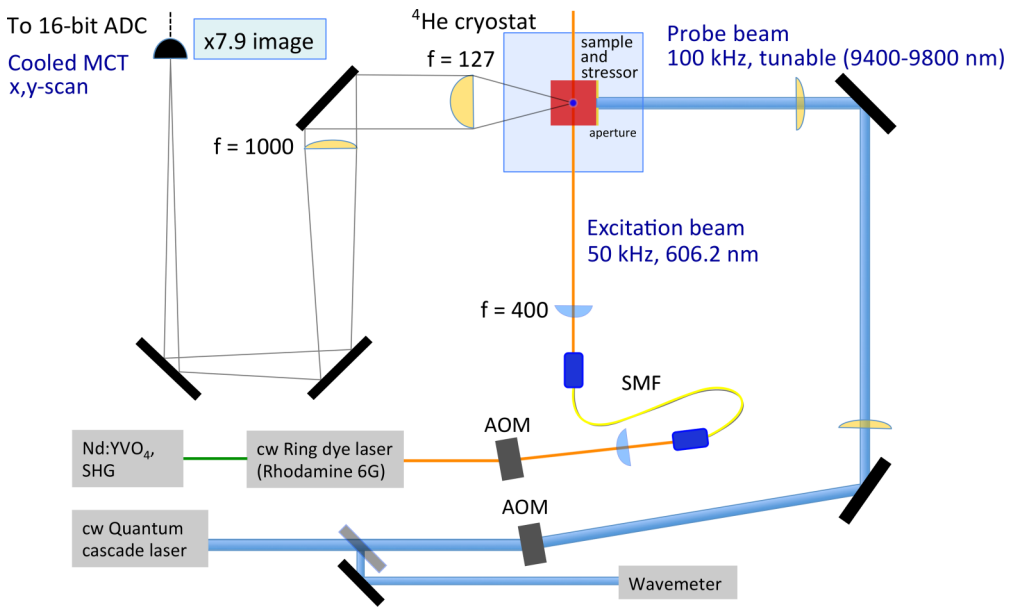

FIG. 2. (Color online) Setup for absorption imaging of trapped yellow-series $1s$ paraexcitons in Cu_2O. We used ZnSe lenses in midinfrared optical paths for ease of alignment. A midinfrared wave meter monitors the oscillating wavelength of a quantum cascade laser. AOM, SMF, and MCT stand for acousto-optic modulator, single-mode fiber, and mercury cadmium telluride detector, respectively.

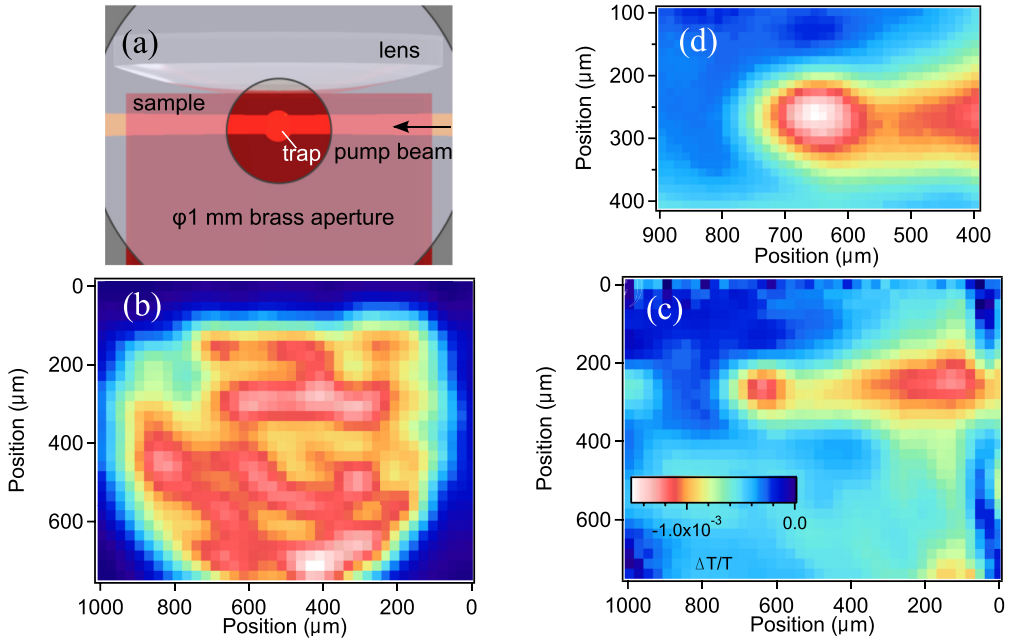

FIG. 3. (Color online) (a) Schematic of a 1-mm-diameter aperture for midinfrared probe light, and the position of the excitation beam. (b) Spatial distribution of the probe-light intensity at 9760 nm. (c) Spatial distribution of the differential transmission. (d) A finer scan near the maximum signal in (c). The maximum induced transmission change is $\Delta T/T = -1.24 \times 10^{-3}$.

cadmium telluride, MCT) photodiode (the active area of which was 0.5×0.5 mm^2) to make a two-dimensional probe intensity and induced absorption distribution. We estimated the spatial resolution to be 80 μm, which was determined by the numerical aperture of the lens and the size of the detector. Acousto-optic modulators chopped the excitation and probe beams at repetition rates of 50 and 100 kHz, respectively (the duty ratios were 50%). A 16-bit analog-to-digital converter recorded every voltage signal from the MCT detector synchronously. A detectable transmission change of 10^{-5} could be achieved in one second. While measuring the induced absorption spectrum at the position of interest, we calibrated the wavelength of the probe beam simultaneously using a midinfrared wave meter.

In Fig. 3, we show a typical intensity distribution of the probe light and the corresponding differential transmission image that were taken at a probe wavelength of 9760 nm (127.0 meV). Figure 3(a) roughly depicts the position of the excitation beam and the stressor lens. We placed the aperture such that it covered the whole trap region. The excitation beam penetrated near the bottom of the trap and generated 1s orthoexcitons mostly in the trap potential. The orthoexcitons converted into paraexcitons and drifted towards the bottom of the trap, where they accumulated. The intensity image of the probe light [Fig. 3(b)] consists of a contour due to the edge of the sample and the aperture, but mostly a fluctuation pattern that originated from multiple reflections at cryostat windows and the sample. Conversely, the differential transmission image [Fig. 3(c)] shows a clear localized signal that suggests the spatial distribution of a trapped paraexciton gas. Figure 3(d) is a two-times-finer differential transmission image of the region of interest in Fig. 3(c).

To prove that the signal is the absorption image of trapped paraexcitons, we first compared its spatial spread with that estimated from a spatially resolved luminescence spectrum that we took simultaneously (paraexcitons with a wave number $k = k_0$ exist with sufficient probability at temperatures of several Kelvin). The spatial distribution (in the vertical direction) at the peak energy of 2.0198 eV is shown in Fig. 4(c). The spatial width (FWHM) was $w_V^{lum} = 121$ μm, which was compared with $w_V = 125$ μm (the spatial resolution shown above was taken into account) in the midinfrared image [see Fig. 4(b)]. The reasonable agreement between the two measurements supports the successful detection of an absorption image of trapped paraexcitons. In addition, the midinfrared image gave the spatial width (FWHM) in the horizontal direction as $w_H = 216$ μm. One can also evaluate w_H from w_V above by comparing vertical ($f_V = 23$ MHz) and horizontal ($f_H = 17$ MHz) trap frequencies and by assuming quasiequilibrium for the trapped exciton gas. The result is $w_H^{calc} = 230$ μm, which is in good agreement with the experimentally determined aspect ratio. Taking into account the steepness of the trap potential, these spatial widths suggest an exciton temperature of 7.0 K.

To find further proof of the absorption imaging, we measured the position dependence of the differential transmission spectrum, since no position dependence was expected for the 1s-2p resonance energy in a strain-free sample. Figures 4(d)–4(f) show the induced absorption spectrum at 0, 130, and 260 μm to the right of the maximum position in the induced absorption image [Fig. 4(a)]. Conversely, the peak energy of the 1s-2p induced absorption spectrum was 128.2 meV at 5 K in a strain-free sample [17]. It follows that the peak energy exhibited a redshift of about 1 meV at maximum.

Since the 1s paraexciton level underwent a redshift in the strain-induced trap, the redshift in the 1s-2p resonance suggests a further redshift for the 2p level. A qualitative consideration can support a large redshift of the 2p level. The

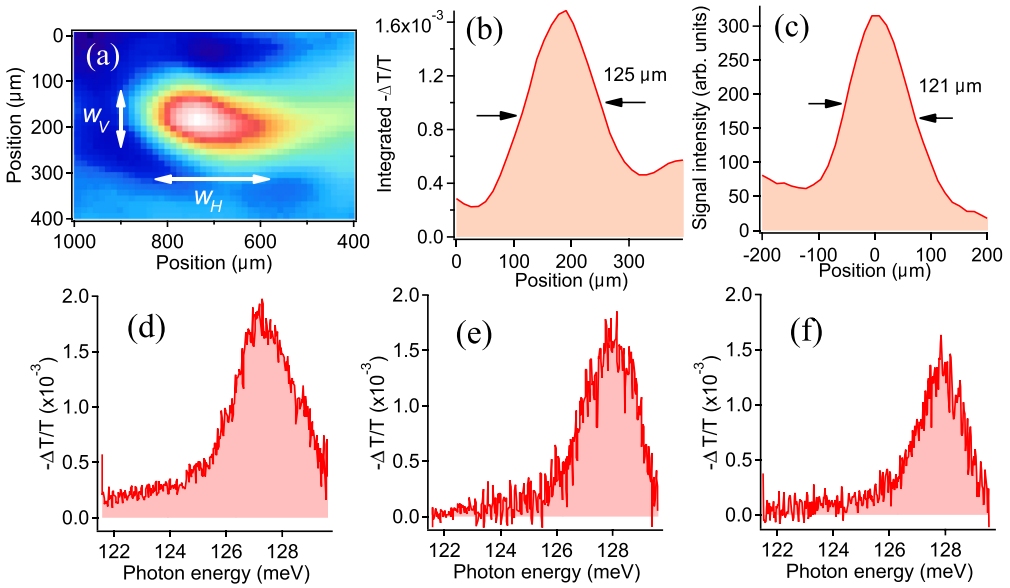

FIG. 4. (Color online) (a) Differential transmission image at a probe wavelength of 9760 nm (the indicated temperature of the cryostat was 2.4 K). (b) Spatial distribution of (a) in the vertical direction (averaged in the horizontal direction). The spatial width (FWHM) is $w_V = 125\ \mu$m. (c) Spatial distribution in the vertical direction that was extracted from the spatially resolved luminescence spectrum. The spatial width (FWHM) is 121 μm. The increasing tail on the left side is due to the Γ_3^--phonon-assisted luminescence of $1s$ orthoexcitons near the rim of the trap potential. We subtracted this contribution when estimating the spatial width. (d)–(f) Probed position dependence of the $1s$-$2p$ paraexciton induced absorption spectrum, (d) at the position where the induced absorption was maximal, (e) at 130 μm, and (f) at 260 μm to the right from (d). The peak energy for a strain-free case is 128.2 meV.

yellow-series excitons are mixed with green-series excitons under a strain field. $1s$ excitons are split (12 meV for the yellow series, and 10 meV for the green series in a strain-free crystal) by the electron-hole exchange interaction, but it is zero for $2p$ excitons. Therefore, second-order perturbation theory gives different energy shifts for the $1s$ and $2p$ levels. In addition, the symmetry of the envelope functions influences the energy shift. Our tentative calculation shows that the yellow-series $2p$ paraexciton levels split into essentially two branches, with one showing a larger redshift than that of the $1s$ paraexciton level and the other exhibiting a blueshift. Consequently, the $1s$-$2p$ paraexciton resonance splits into two types of branches, one with a small redshift (which was observed here) and the other with a relatively large blueshift. Due to the position-dependent shift in the $1s$-$2p$ resonance energy, a careful treatment is required to analyze the induced absorption spectrum for spatially spread excitons in a trap. We will give a detailed discussion of the spectral line-shape analysis in a forthcoming paper.

Finally, an important aspect of our technique is its capability to measure the absolute density of $1s$ paraexcitons. As discussed above, the $1s$-$2p$ offset energy in the trap is dependent on the position. However, by taking the spectrally integrated $\Delta\alpha_{1s-2p}$, such a spectral structure becomes unimportant and only the position dependence of the exciton density remains. The average density of paraexcitons in a probed region is expressed in the following equation:

$$n_{1s} = \frac{\hbar c \epsilon_0 n}{\pi |\mu_{1s-2p}|^2 E_{1s-2p}} \int \Delta\alpha_{1s-2p}(E) dE, \qquad (1)$$

where ϵ_0 is the dielectric constant in vacuum, n is the index of refraction of Cu_2O in the midinfrared region, μ_{1s-2p} is the transition dipole moment, and E_{1s-2p} is the $1s$-$2p$ offset energy. To evaluate the differential absorption coefficient $\Delta\alpha_{1s-2p}(E)$ from the differential transmission $\Delta T/T(E)$, one needs to know the size (w_D) of the exciton cloud in the direction of the probe laser beam, since $\Delta\alpha_{1s-2p}(E) = -\ln[\Delta T/T(E) + 1]/w_D$. The density distribution is Gaussian in the present quasiequilibrium condition. By applying the reasonable assumption that w_D was the same as the horizontal width w_H because the trap frequencies for both directions are the same, the average density was found to be $n_{1s} = 2.3 \times 10^{13}$ cm^{-3} when we probed the center of the trapped gas as in Fig. 4(d). We believe that the error of the density estimate is $\pm 20\%$, which originates from the error in the estimated transition dipole moment ($\mu_{1s-2p} = 3.5 \pm 0.3$ eÅ [1]).

For comparison, we could roughly calculate the average density from the absorbed optical power and the spatial spread of w_V and w_H, on the basis of the rate equation,

$$\frac{d}{dt} n_{1s} = -\frac{n_{1s}}{\tau} - A n_{1s}^2 + \frac{G}{V_{avg}}. \qquad (2)$$

$\tau = 300$ ns is the measured lifetime of $1s$ paraexcitons, $A = 4 \times 10^{-16}$ cm^3/ns [1] is the two-body collision-induced loss coefficient (an identical value to that in the unstressed sample is assumed here), $G = 2.7 \times 10^6$ excitons/ns is the generation rate (a 30% [6] efficiency is assumed for the capturing of $1s$ paraexcitons in the trap potential after the creation of $1s$ orthoexcitons), and $V_{avg} = w_H \times w_H \times w_V = 5.8 \times 10^{-6}$ cm^3 is the average volume. The calculated steady-state, average density is $n_{1s} = 3.0 \times 10^{13}$ cm^{-3}, demonstrating the quantitativeness of the present technique.

Future extension of the present technique to sub-100-mK temperatures might be hampered by unwanted thermal radiation. The $1s$-$2p$ resonance wavelength lies in the center of

the spectrum of the blackbody radiation at room temperature, so that incoming thermal flow makes 100 mK experiments difficult. The use of narrow bandpass filters as windows for a radiation shield in a cryostat and proper limitation of their aperture sizes will solve this problem. In fact, in our preliminary experiment, we have already achieved a temperature of about 120 mK while transmitting a midinfrared beam.

To summarize, we have demonstrated the absorption imaging of trapped excitons in a bulk semiconductor using midinfrared absorption associated with an excitonic 1s-2p transition. The spatial size of the clear absorption image coincided with what we could measure in luminescence experiments. The induced absorption spectra exhibited position-dependent redshifts that could not be observed in a strain-free sample. These results provide evidence of a successful detection of an absorption image of 1s paraexcitons in a trap potential. A relatively dilute gas with an average density of 2×10^{13} cm^{-3} was clearly detected with a sufficient signal-to-noise ratio. Considering that the BEC critical density is 9×10^{14} cm^{-3} at 100 mK, this result demonstrates that this technique is of sufficient sensitivity to capture a dark and quantum degenerate exciton gas at sub-Kelvin temperatures. It will be especially useful for detecting characteristic changes in spatial and spectral distributions upon transition to a BEC. Due to its quantitative nature, the absorption imaging will be of great importance for better understanding characteristic phenomena that have been reported, such as superfluiditylike ballistic transport [24] and relaxation explosion [6] at the BEC phase transitions seen at higher temperatures. Extension to time-resolved studies using a pulsed quantum cascade laser will contribute to a complete understanding of ultracold quantum statistical excitons in a trap.

The authors would like to thank E. Chae for fruitful discussions and H. Sakurai and Y. Aratake for supporting the initial stage of this work. This work was supported by a Grant-in-Aid for Young Scientists (A) (Grant No. 25707024), Grant-in-Aid for Scientific Research (A) (Grant No. 26247049), the Photon Frontier Network Program of the Ministry of Education, Culture, Sports, Science and Technology (MEXT), Japan, and the Project for Developing Innovation Systems of MEXT.

[1] K. Yoshioka, T. Ideguchi, A. Mysyrowicz, and M. Kuwata-Gonokami, Phys. Rev. B **82**, 041201(R) (2010).
[2] K. E. O'Hara and J. P. Wolfe, Phys. Rev. B **62**, 12909 (2000).
[3] J. I. Jang and J. P. Wolfe, Phys. Rev. B **74**, 045211 (2006).
[4] J. P. Wolfe and J. I. Jang, New J. Phys. **16**, 123048 (2014).
[5] D. W. Snoke and G. M. Kavoulakis, Rep. Prog. Phys. **77**, 116501 (2014).
[6] K. Yoshioka, E. Chae, and M. Kuwata-Gonokami, Nat. Commun. **2**, 328 (2011).
[7] D. P. Trauernicht, J. P. Wolfe, and A. Mysyrowicz, Phys. Rev. B **34**, 2561 (1986).
[8] N. Naka and N. Nagasawa, Phys. Rev. B **70**, 155205 (2004).
[9] K. Yoshioka, Y. Morita, K. Fukuoka, and M. Kuwata-Gonokami, Phys. Rev. B **88**, 041201 (2013).
[10] H. Stolz, R. Schwartz, F. Kieseling, S. Som, M. Kaupsch, S. Sobkowiak, D. Semkat, N. Naka, T. Koch, and H. Fehske, New J. Phys. **14**, 105007 (2012).
[11] S. Sobkowiak, D. Semkat, and H. Stolz, Phys. Rev. B **90**, 075206 (2014).
[12] M. Kuwata-Gonokami, M. Kubouchi, R. Shimano, and A. Mysyrowicz, J. Phys. Soc. Jpn. **73**, 1065 (2004).
[13] M. Jörger, T. Fleck, C. Klingshirn, and R. von Baltz, Phys. Rev. B **71**, 235210 (2005).
[14] T. Tayagaki, A. Mysyrowicz, and M. Kuwata-Gonokami, J. Phys. Soc. Jpn. **74**, 1423 (2005).
[15] R. Huber, B. A. Schmid, Y. R. Shen, D. S. Chemla, and R. A. Kaindl, Phys. Rev. Lett. **96**, 017402 (2006).
[16] S. Leinß, T. Kampfrath, K. von Volkmann, M. Wolf, J. T. Steiner, M. Kira, S. W. Koch, A. Leitenstorfer, and R. Huber, Phys. Rev. Lett. **101**, 246401 (2008).
[17] K. Yoshioka and M. Kuwata-Gonokami, New J. Phys. **14**, 055024 (2012).
[18] M. H. Anderson, J. R. Ensher, M. R. Matthews, C. E. Wieman, and E. A. Cornell, Science (NY) **269**, 198 (1995).
[19] C. C. Bradley, C. A. Sackett, J. J. Tollett, and R. G. Hulet, Phys. Rev. Lett. **75**, 1687 (1995).
[20] K. B. Davis, M. O. Mewes, M. R. Andrews, N. J. van Druten, D. S. Durfee, D. M. Kurn, and W. Ketterle, Phys. Rev. Lett. **75**, 3969 (1995).
[21] J. Brandt, D. Fröhlich, C. Sandfort, M. Bayer, H. Stolz, and N. Naka, Phys. Rev. Lett. **99**, 217403 (2007).
[22] K. Yoshioka, T. Ideguchi, and M. Kuwata-Gonokami, Phys. Rev. B **76**, 033204 (2007).
[23] J. Brandt, P. Felbier, D. Fröhlich, C. Sandfort, M. Bayer, and H. Stolz, Phys. Rev. B **81**, 155214 (2010).
[24] E. Fortin, S. Fafard, and A. Mysyrowicz, Phys. Rev. Lett. **70**, 3951 (1993).